

Employing the Local Radon Transform for Melanoma Segmentation in Dermoscopic Images

Abstract

In recent years, the number of patients suffering from melanoma, as the deadliest type of skin cancer, has grown significantly in the world. The most common technique to observe and diagnosis of such cancer is the use of noninvasive dermoscope lens. Since this approach is based on the expert ocular inference, early stage of melanoma diagnosis is a difficult task for dermatologist. The main purpose of this article is to introduce an efficient algorithm to analyze the dermoscopic images. The proposed algorithm consists of four stages including converting the image color space from the RGB to CIE, adjusting the color space by applying the combined histogram equalization and the Otsu thresholding-based approach, border extraction of the lesion through the local Radon transform, and recognizing the melanoma and nonmelanoma lesions employing the ABCD rule. Simulation results in the designed user-friendly software package environment confirmed that the proposed algorithm has the higher quantities of accuracy, sensitivity, and approximation correlation in comparison with the other state-of-the-art methods. These values are obtained 98.81 (98.92), 94.85 (89.51), and 90.99 (86.06) for melanoma (nonmelanoma) lesions, respectively.

Keywords: Cancer, dermoscopic images, image processing, lesion, melanoma, segmentation

Introduction

Skin cancer is known as the most common and deadly diseases in the world. Based on a study done in the United States, about 20% of people suffer from this cancer during their life.^[1] Skin cancer can be categorized as melanoma and nonmelanoma ones. Melanoma is considered as the most dangerous type of skin cancer. Following to the World Health Organization report, approximately 70,230 people die every year because of the melanoma.^[2] The origin of this cancer is in the skin epidermis and dermal layers. It forms from the accumulation of melanin seeds and its propagation to the outer layer of the skin. The nonmelanoma skin cancer generally begins in the basal or squamous cells. Direct sunlight exposure on the skin is the main factor of growing the basal cells. These kind of cancerous cells are completely treatable in the early stage of diagnosis.^[2]

The first dermoscope setup was invented by Goldman in 1951 to evaluate the deviations in the skin pigmentation disorders.^[3] After

that, dermatologists used this device as a suitable non-invasive tool for the skin lesions observation. By developing the technology, the digital versions of dermoscope with the ability of receiving and storing the skin images are replaced with the conventional ones. In such a device, by designing some appropriate filters, it is possible to remove the reflected or rescattered nonpolarized lights. During the imaging, the pigmentation of the lesion on the skin is coated with an oil or alcohol liquid that leads to reduce the skin reflections.^[3,4]

Computer-aided diagnosis (CAD) has a vital role to measure a set of features in the dermoscopic images (DIs).^[5] CAD has a significant contribution to the dermatologists to diagnose the skin cancer in its early stage. To detect a skin lesion, a deep understanding of the various dermoscopic features associated with cancer, including individual patterns of a lesion such as the color and symmetry, is an important issue. The common configuration of a dermoscopic CAD includes four stages: preprocessing, segmentation, feature extraction, and classification. Among them, segmentation is the most difficult step in the CAD due to the following:

How to cite this article: Amoabedini A, Farsani MS, Saberkari H, Aminian E. Employing the local Radon transform for melanoma segmentation in dermoscopic images. *J Med Sign Sens* 2018;8:184-94.

**Alireza
Amoabedini¹,
Mahsa Saffari
Farsani²,
Hamidreza
Saberkari³,
Ehsan Aminian¹**

¹Department of Computer Engineering, Safadasht Branch, Islamic Azad University, Tehran, Iran, ²Department of Electrical Engineering, Yazd University, Yazd, Iran, ³Department of Electrical Engineering, Sahand University of Technology, Tabriz, Iran

A. Amoabedini

ORCID ID

<https://orcid.org/0000-0002-5891-1582>

Address for correspondence:

Mr. Alireza Amoabedini,
Department of Computer
Engineering, Safadasht Branch,
Islamic Azad University, Tehran,
Iran.

E-mail: amoabedini@safaiau.ac.ir

Website: www.jmss.mui.ac.ir

DOI: 10.4103/jmss.JMSS_40_17

This is an open access journal, and articles are distributed under the terms of the Creative Commons Attribution-NonCommercial-ShareAlike 4.0 License, which allows others to remix, tweak, and build upon the work non-commercially, as long as appropriate credit is given and the new creations are licensed under the identical terms.

For reprints contact: reprints@medknow.com

- (i) It directly affects the accuracy of the other steps
- (ii) The transition from a lesion to a healthy area is often accompanied by a low contrast
- (iii) The lesion borders usually have a fuzzy behavior and do not follow a particular regularity and
- (iv) The presence of artifacts has a negative impact in the segmentation accuracy.

There are some works presented in the literature for the melanoma lesion segmentation in the DIs. In a method proposed by Emre Celebi *et al.*^[6] a seeded region growing was rendered that initiates with a selection of a pixel as the starting seed. Afterward, the seeds are aggregated utilizing two criteria, homogeneity and adjacency. Proper selection of the initial seeds is a vital issue in this method. In a study by Fondn *et al.*,^[7] this was done using the mouse, as the starting point and stopping criterion can be determined in a good manner. In a study by Amalian *et al.*,^[8] a method was rendered based on the selection of the center of a homogeneous area as the starting seed, and then, regulating a threshold level randomly. The methods proposed by Fondn *et al.*^[7] and Amalian *et al.*^[8] have a poor segmentation accuracy owing to adjusting the parameters manually. To solve this restriction, a method was presented in a study by Smaoui and Bessassi^[9] to adaptively select the starting point as well as the threshold level. Furthermore, for each level of growth, the adjacent pixels with similar properties are added to the image. With regard to the fact that the lesion is always darker than the healthy area of the skin, the seed pixel is adaptively selected as a pixel with a gray-scale level that has a high similarity to its neighboring pixels. This characteristic is achieved by calculating the Euclidian or Manhattan distances between a sample pixel and the 5×5 window of its neighboring pixels.

In a study by Grana *et al.*,^[10] lesion borders were extracted using the mathematical descriptors. In this method, first, two new descriptors, the slope of the lesion and the regulation degree of the lesion slope, are modeled mathematically. Afterward, lesion borders are recognized through a new algorithm based on the Catmull–Rom spline interpolation. In this method, the gray-level gradient of the extracted points is calculated by employing the spline interpolation in the perpendicular direction of the spline.

In a study by Ammara *et al.*,^[11] a thresholding-based approach was presented to melanoma lesion segmentation. In this approach, first, the melanoma image is segmented automatically by applying the Otsu thresholding method, and then, k points are selected to apply the spline-based interpolation. This approach has suitable performance in the case of the contrast between the lesion and skin is appropriate. Nevertheless, the lesion and skin regions usually have overlaps in the DIs. This issue can be solved using the edge(area)-based segmentation techniques. In a method proposed by Rubegni *et al.*^[12] and Zhou *et al.*,^[13] segmentation of the DIs was conducted by employing the

Laplacian of Gaussian operator and active contour model, respectively.

In a study by Stoecker *et al.*,^[14] the granular regions were recognized by extracting 10 and 22 features which are related to the texture and color of the DIs. Some color features are: the mean quantities of RGB pixels, the relative mean values of each RGB pixels ($relR$, $relG$, $relB$), the absolute values of RGB chromaticity, the mean value of G/B , the mean value of $relG/relB$, the luminance value that is defined as $luminance = 0.30 R + 0.59 G + 0.11 B$, and the variance of R . In addition, some texture features are the average values of energy, inertia, correlation, and entropy.

In a study by Dalila *et al.*,^[15] by defining three types of features, geometrical, texture, and relative colors, the authors proposed an automated system based on the Ant colony segmentation algorithm. Although the Ant colony is an inherent parallelism approach which could be adapted to changes such as new distance; however, its probability distribution will be changed by iteration.

Skin cancer diagnosis based on deep neural network is utilized in a study by Zhang^[16] which is able to improve the efficacy for identification of normally indistinguishable lesions versus clinically unknown lesions. Results demonstrate that the neural network architecture achieves higher accuracy for segmentation of melanoma images as compared with existing processes. However, this improvement leads to increase the computational complexity due to high training time of the deep neural network.

In a method proposed by Pennisi *et al.*,^[17] Delaunay Triangulation is used to extract a binary mask of the lesion region, without the need of any training stage. This algorithm uses different parameters to carry out the segmentation; however, most of them are related to the size of the images in input and to the considered skin types, thus they can be predefined.

A novel approach based on deformable model is proposed in a study by Ma and Tavares^[18] to automatically segment the skin lesions. The proposed algorithm combines the information contained in DIs and defines the speed function based on the lightness, saturation, and color information. However, this study does not consider the influence of shape feature on the classification of the skin lesions.

In this article, we propose a new algorithm to melanoma segmentation that consists of four main stages [Figure 1]: (i) converting the image color space, (ii) histogram equalization and adjusting the color space and the image contrast enhancement, (iii) border extraction of the lesion by applying the local Radon transform (LRT), and (iv) melanoma and nonmelanoma lesions recognizing using the ABCD rule. To the best of our knowledge, this is the first attempt for the melanoma segmentation utilizing the LRT algorithm. In the following, Section 2 contains the

main steps of the proposed algorithm. Simulation results in the designed user-friendly software package environment are rendered in Section 3, and finally, Section 4 includes the conclusion of the paper.

Proposed Algorithm

Image color space conversion

One way to increase the contrast of an image refers to transferring of it to a new space, in which the image intensity is directly related to its main components.^[19] To this end, first, we transfer the image color space from the RGB to CIE (L^*a^*b), and then, the remaining processes are done in the sublayer L . Regulating the sublayer L affects the intensity of the pixels, while it maintains the original color of the image. The pixel quantities in this sublayer are set in the range of 0–100. To yield the appropriate image contrast, we set the intensity range of the pixels in accordance with the lesion and background contrasts based on the Otsu thresholding algorithm.^[20] The Otsu thresholding is a method to segment an image based on the proper selection of an optimal threshold level t , as it creates the maximum uniformity in the intensity function of each classes, and concurrently, it minimizes the variance of the intensity function between the classes. We can write:

$$\sigma_w^2(t) = \omega_1(t) \cdot \sigma_1^2(t) + \omega_2(t) \cdot \sigma_2^2(t) \quad (1)$$

Where the weights ω_i are the occurrence probabilities of the two classes separated by the threshold level t and σ_i^2 is the variance of these classes. Minimizing the between-class variance is described through the occurrence probability of each class (ω_i) and the class average ($\mu_i(t)$) based on the following condition:

$$\sigma_b^2(t) = \sigma^2 - \sigma_w^2(t) = \omega_1(t) \cdot \omega_2(t) (\mu_1[t] - \mu_2[t])^2 \quad (2)$$

The occurrence probability and the average of the class 1 are calculated as relations (3) and (4), respectively.

$$\omega_1(t) = \sum_{i=0}^t p(i) \quad (3)$$

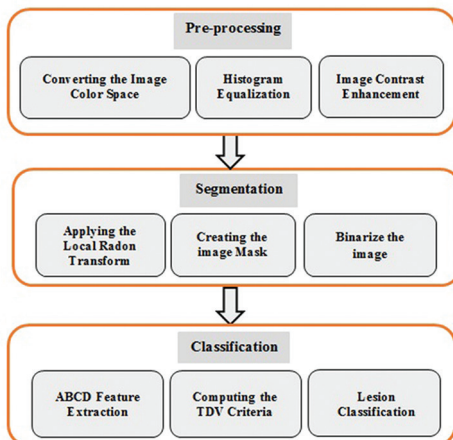


Figure 1: Block diagram of the proposed algorithm

$$\mu_1(t) = \frac{\sum_{i=0}^t p(i) \cdot x(i)}{\omega_1} \quad (4)$$

where $x(i)$ is the preset value in the center of i^{th} level of histogram. The values of $\omega_2(t)$ and $\mu_2(t)$ are calculated similarly. After obtaining the optimal threshold level, we apply it to the sublayer L in the CIE color space.

Based on the Otsu thresholding, if the variance between the lesion and the background is high, the image intensity range should be smaller to leave out the probable lesions with lower luminance. On the other hand, in the case of small variance among the lesion and the background, the image intensity range should be considered large enough to preserve the lesion details. Consequently, the range of pixel intensities in this sublayer is divided by the Max Luminosity defined as Eq. 5. Figure 2a depicts the result of applying the proposed color space conversion to a sample DI.

$$\text{Max Luminosity} = \begin{cases} 5 & \text{if } t < 0.5 \\ 10 & \text{if } 0.5 < t < 0.6 \\ 50 & \text{if } t > 0.6 \end{cases} \quad (5)$$

Histogram equalization and contrast enhancement

The second step consists of the histogram equalization and image contrast enhancement. Adjustment of the image histogram is a common technique to set the image intensities, resulting in contrast improvement. The goal of this step is to reduce the background noise as to determine the focal regions in the DIs. More details of the histogram equalization are referred from the study by Singh and Dixit.^[21] After equalizing the histogram, the obtained image is multiplied again in the parameter Max Luminosity

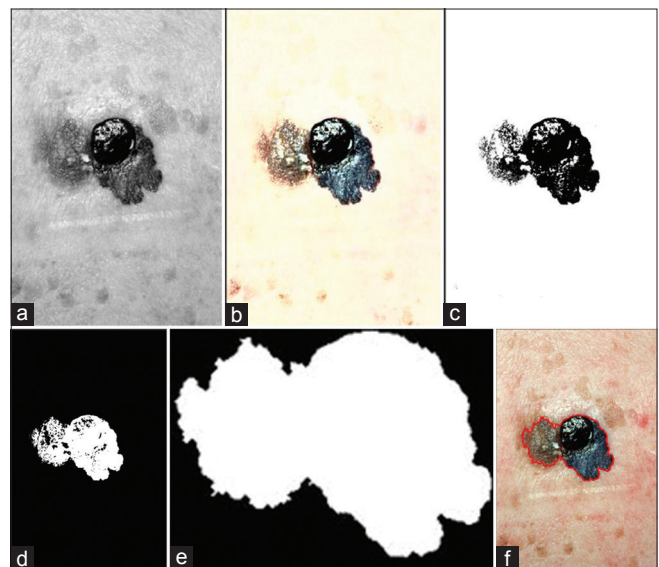


Figure 2: Results of the different steps of the proposed algorithm for a sample dermoscopic image (a) color space conversion, (b) histogram equalization, (c) contrast enhancement, (d) applying the local Radon transform, (e) filling the holes, (f) determining the lesion border



Figure 3: (a-j) Results of applying the proposed algorithm for ten dermoscopic samples containing melanoma lesion

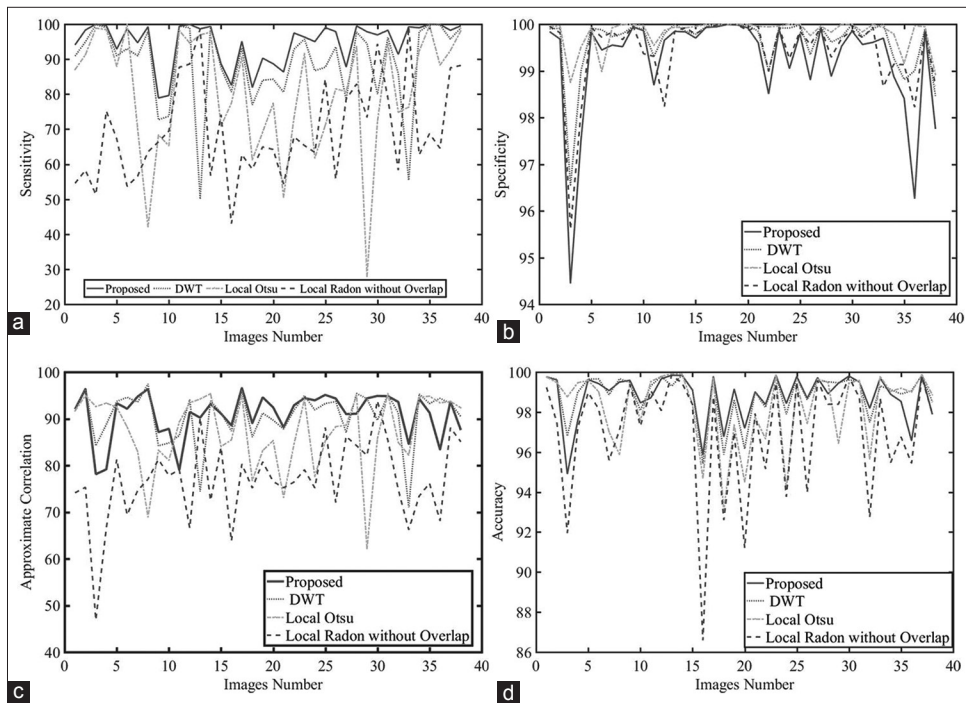


Figure 4: The curves of (a) sensitivity, (b) specificity, (c) approximation correlation, and (d) accuracy in the proposed algorithm and the other tested methods for 38 dermoscopic samples containing melanoma lesion

defined in Eq. 5 to keep the color intensities in the range of 0–100. Figure 2b shows the result of histogram equalization for a sample DI.

In the next step, the image contrast enhancement is performed. In many DIs, the background and foreground regions have a low contrast despite employing the color space conversion and histogram equalization. Hence, the

goal of the contrast enhancement step is to emboss the embedded features in the image. In this regard, we employ the method proposed by Shao *et al.*^[22] for enhancing the image contrast. Let $f(x, y)$ represents a DI in which $x \in (1, w)$ and $y \in (1, h)$ demonstrate the image width and height, respectively. A 2D image is projected into 1D signal, as denoted by p , and the contrast enhanced image g is calculated using Eq. 6.

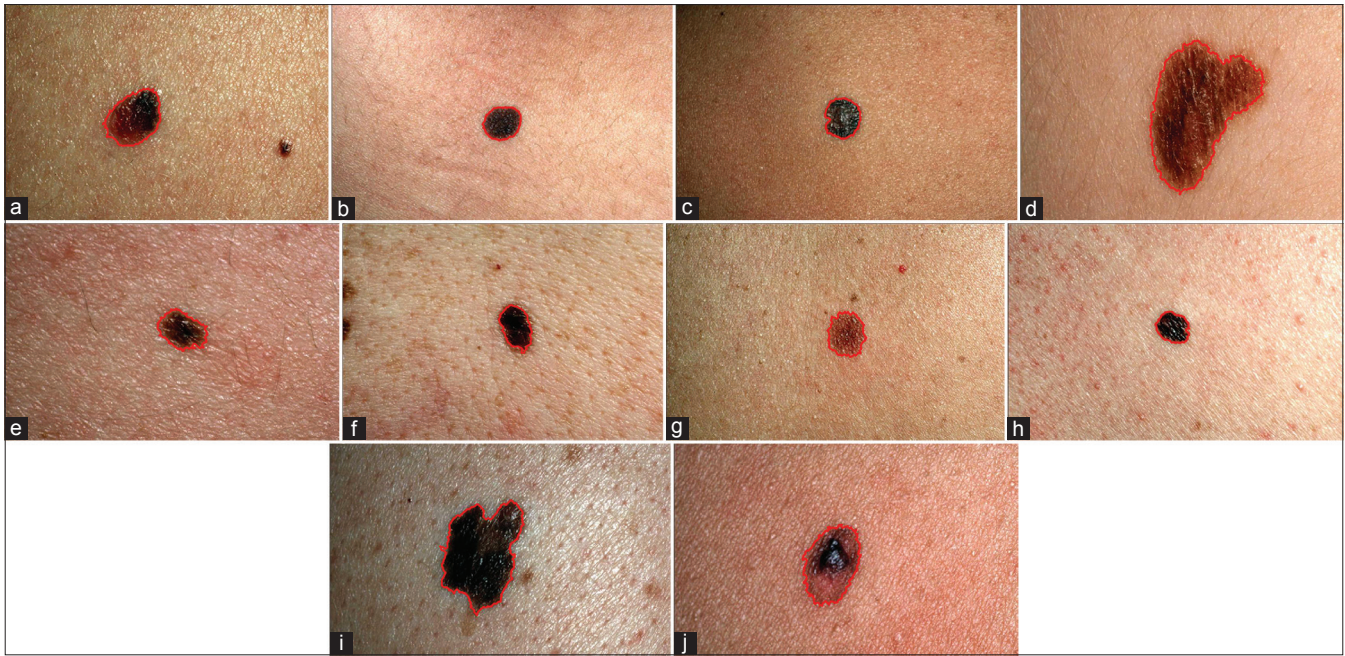


Figure 5: (a-j) Results of applying the proposed algorithm for ten dermoscopic samples without melanoma lesion

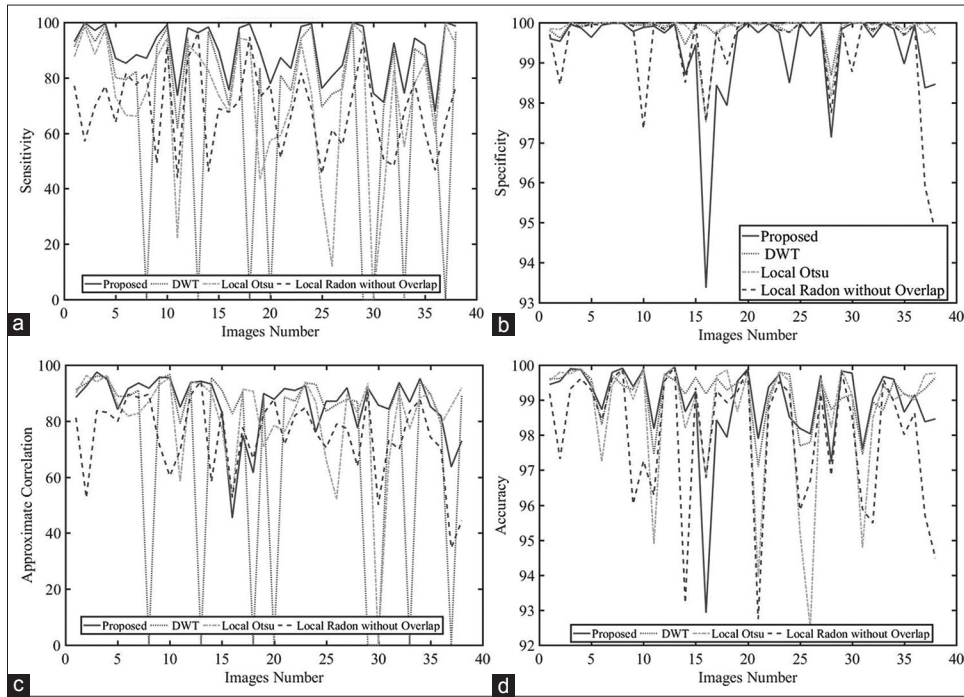


Figure 6: The curves of (a) sensitivity, (b) specificity, (c) approximation correlation, and (d) accuracy in the proposed algorithm and the other tested methods for 38 dermoscopic samples without melanoma lesion

$$g(x, y) = \begin{cases} f(x, y) \times \left(\frac{1000}{C}\right) & f(x, y) > k \\ f(x, y) & o.w \end{cases} \quad (6)$$

where C is the degree of the contrast enhancement and set automatically as:

$$C = \frac{s}{\left[\left(\frac{s^4}{s^2}\right)^2\right]^{\frac{1}{4}}} \quad (7)$$

In the above equation, $s = \left[\frac{1}{N} \sum (p - \bar{p})^2\right]^{\frac{1}{2}}$, $s^4 = \left[\frac{1}{N} \sum (p - \bar{p})^4\right]$ and $s^2 = \frac{1}{N} \sum (p - \bar{p})^2$. Furthermore, $\bar{p} = \frac{1}{N} \sum p$ is the average value, s denotes the standard deviation, s^2 represents the variance, and s^4 is the fourth-order momentum. Figure 2c shows the contrast enhancement result for a sample DI.



Figure 7: The quantities of ABCD features and the result of total dermoscopy score criteria for the four dermoscopic samples with melanoma

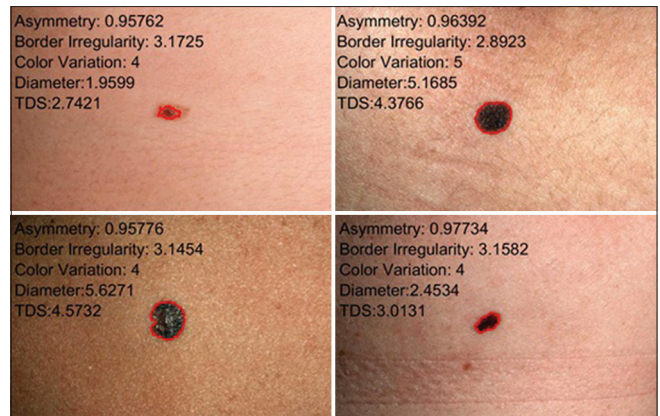


Figure 8: The quantities of ABCD features and the result of total dermoscopy score criteria for the four dermoscopic samples without melanoma



Figure 9: The designed user-friendly software package to classify the skin lesions into the benign, suspicious, and melanoma (the recognition result: melanoma (cancer) lesion)

Border extraction of the skin lesions by applying the local Radon transform

In the next step, the high-quality image is processed by applying the RT to estimate the probable line angle. The RT of a 2D image $g(x, y)$ is defined as below:^[23]

$$\tilde{g}(\rho, \theta) = \int_{-\infty}^{\infty} \int_{-\infty}^{\infty} I(x, y) \delta(\rho - x \cos \theta - y \sin \theta) dx dy \quad (8)$$

Where $I(x, y)$ represents the gray-scale intensity of the image in the pixel (x, y) . Furthermore, $\delta(\cdot)$ is the Dirac delta function. In the RT space, the intensity of each pixel with the coordinates of (ρ, θ) corresponds to the integral of the image over a straight line with an angle of θ relative to the x -axis and a distance ρ from the origin.

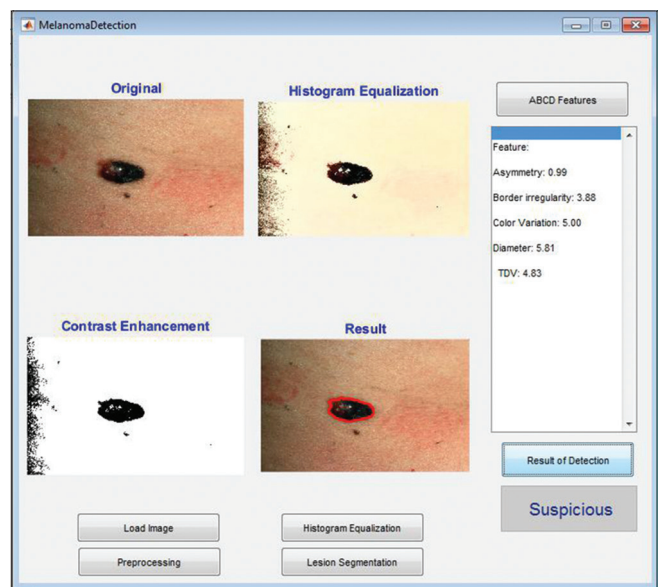


Figure 10: The designed user-friendly software package to classify the skin lesions into the benign, suspicious, and melanoma (the recognition result: suspicious lesion)

The gray-scale image resulted from the contrast enhancement step indicates an appropriate approximate version of the desired skin lesion. However, the key point to recognize the cancerous moles in such images is to accurate extraction of their borders, due to the irregular nature of the melanoma. To this end, in this article, we employ the LRT,^[24] in which first, the entire image divides into the overlapping windows, and then, the RT is applied to each subwindow. This modification leads to reduce the probability error in the line detection in different angles compared to the RT without overlapping. To locate the RT, the square window with the length of $n = 100$ and the pitch size of $n/3$ slides along the horizontal and vertical directions on the image. The disadvantage of the square window is its larger diameter relative to the side that leads to increase the occurrence probability of the maximum of RT over the diagonal direction with the degree of 45. To solve this restriction, we apply a circular mask with the radius of $n/2$ to each window.

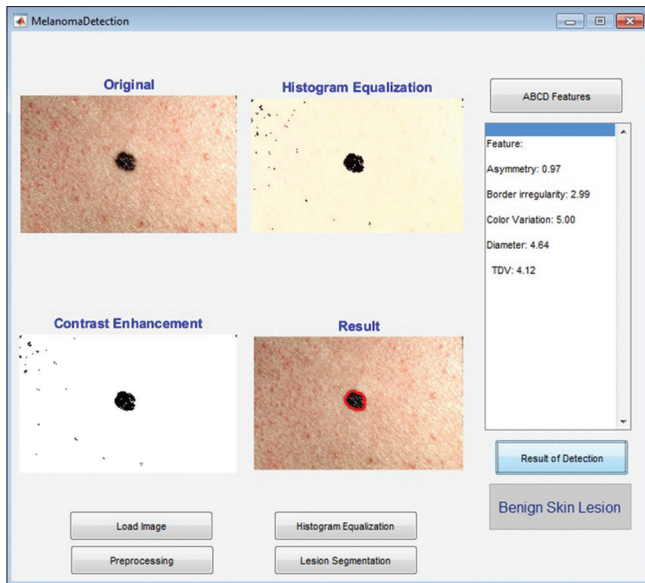


Figure 11: The designed user-friendly software package to classify the skin lesions into the benign, suspicious, and melanoma (the recognition result: benign lesion)

The RT is based on the image projection for different angles. The projected signals with the range of 0° – 180° have the maximum value in the angle corresponding with a probable lesion border. Consequently, by applying the RT in each window, a column that has the maximum quantity in its corresponding sinogram space outlines the angle of the line. After determining the line angle, a binarized mask should be created at this angle based on the following procedure: if we assume that there is a lesion border in the corresponding window, both the lesion border and the background pixels can be affected on the amplitude of the projected signal.^[24] For normalization, first, the average of pixels intensity of the corresponding window should be subtracted from the projected signal. In the case that there is no lesion in a window, this difference will be zero and the mask will be totally black; otherwise, the initial and the end nonzero points of the i^{th} column are considered as the mask coordinates. Next, the columns distance between the starting and ending points of the mask are set to 1 and the other regions are set to 0 in each window. Afterward, this distance is rotated to the specified angle, and hence, the binary mask will be created. By multiplying the obtained mask into the original image and calculating the average of each region, the original binarized image will be obtained. Finally, to create the binary mask of a lesion, possible holes of the binary image are filled with the white pixels.

One of the differences between the melanoma lesions in comparison with the normal moles is their diameter. More specifically, the lesions with a diameter more than 6 mm are considered as melanoma. Therefore, in the proposed algorithm, we remove the objects with the size <500 pixels

through employing the four-connected component labeling approach. Figures 2d-f depict the results of applying the LRT, binarized image, filling the holes by white pixels, and detecting of the melanoma lesion border.

Skin lesions classification using the ABCD rule

The last step of the proposed algorithm comprises the feature extraction from the segmented image to diagnose the skin lesions. To this end, we conduct the ABCD rule^[25] which was established in 1985 by a group of researchers at the New York University. The ABCD rule includes four components as: (i) asymmetry: it evaluates the results of lesion symmetry, (ii) border: it utilizes to estimate the lesion border, (iii) color: it determines the number of colors in a lesion, and (iv) diameter: the lesions with a diameter more than 6 mm are considered as melanoma. The symmetry feature is the most important indicator in the lesion description and is considered based on the two shape and color parameters. After extracting the four features related to ABCD rule, the total dermoscopy score (TDS)^[9] is calculated based on Eq. 9, in which each of the components is weighted with a coefficient.

$$\text{TDS} = 1.3 \times A + 0.1 \times B + 0.5 \times C + 0.5 \times D \quad (9)$$

Following the TDS criteria, the classification of the skin lesions into benign and malignant can be interpreted as below:

- If $\text{TDS} < 4.75$ the skin lesion will be benign
- If $4.75 \leq \text{TDS} \leq 5.45$ the skin lesion will be suspicious to cancerous cell
- If $\text{TDS} > 5.45$ the skin lesion will be malignant.

Results and Discussion

The proposed algorithm is tested qualitatively on the DIs from two public datasets, the dermatology information system, and DermQuest.^[26] The first dataset contains 43 malignant melanomas and 26 nevi and the second dataset includes 76 malignant melanomas and 61 nevi. In this article, we used the 76 DIs including the border irregularities, low level of contrast, and inappropriate condition of imaging, in which 38 images are related to melanoma lesion and 38 images correspond to nonmelanoma lesion. Each image contains a single lesion of interest, which was manually segmented. The test infrastructure was implemented in MATLAB environment.

Quantitative evaluation of the proposed algorithm is conducted utilizing the sensitivity (S_n), specificity (S_p), precision (P), and approximation correlation (AC) criteria that are defined as follows:^[20]

$$S_n = \frac{TP}{TP + FN} \quad (10)$$

$$S_p = \frac{TN}{TN + FP} \quad (11)$$

$$P = \frac{TP+TN}{TP+FP+TN+FN} \tag{12}$$

$$AC = \frac{1}{4} \left(\frac{TP}{TP+FN} + \frac{TP}{TP+FP} + \frac{TN}{TN+FN} + \frac{TN}{TN+FP} \right) \tag{13}$$

Where TP and TN represent the number of pixels correctly identified as melanoma and nonmelanoma lesions, respectively. Similarly, FP and FN represent the number of pixels incorrectly identified as melanoma and nonmelanoma lesions regions, respectively. We have utilized the above evaluation criteria to assess the correct detection rate. According to Eqs. 10 and 11, the sensitivity parameter provides a measure of melanoma pixels correctly identified as melanoma region. Furthermore, the specificity parameter provides a measure of background pixels correctly detected by the proposed algorithm as the background region. Finally, the precision parameter shows the detection rate of the system.

Table 1 shows the quantitative values of accuracy, specificity, and sensitivity for ten dermatoscopic samples containing melanoma lesion. In this table, *n* represents the nonoverlap window and *n*/10 denotes the 90% overlapping. As it can be seen, the sensitivity increases in accordance with raising the overlapping step. The highest value of the sensitivity corresponds to the sliding step of *n*/10; however, this improvement causes more computational complexity. From Table 1, we can conclude that the sliding step of

Table 1: Quantitative values of accuracy, specificity, and sensitivity for ten dermatoscopic samples containing melanoma lesion

Step	Accuracy (%)			Specificity (%)			Sensitivity (%)		
	<i>n</i>	<i>n</i> /3	<i>n</i> /10	<i>n</i>	<i>n</i> /3	<i>n</i> /10	<i>n</i>	<i>n</i> /3	<i>n</i> /10
NM61_orig	97.4	99.6	99.2	99.91	99.64	99.19	55.14	98.39	98.70
SSM15_orig	99.4	99.4	99.3	99.45	99.47	99.29	97.59	98.54	98.54
SSM18_orig	95.6	99.0	97.9	99.73	99.54	98.29	57.5	94.10	99.89
SSM21_orig	99.4	99.6	99.6	99.96	99.35	99.95	66.38	78.89	78.82
SSM23_orig	98.3	98.3	98.6	99.08	98.32	98.60	55.96	99.34	99.34
SSM31_orig	88.9	96.5	95.4	99.89	99.88	98.46	53.08	85.28	85.52
SSM36_orig	88.1	98.0	97.3	99.90	99.52	98.24	51.14	93.35	94.47
SSM58_orig	94.1	98.0	96.3	99.28	97.85	95.85	58.81	98.68	99.31
SSM62_orig	98.5	98.9	98.6	98.77	98.75	98.51	93.78	99.5	99.65
SSM33_orig	95.9	98.3	98.0	98.14	99.36	97.83	64.63	99.70	99.84

n/3 has the higher sensitivity compared to the nonoverlap window. For instance, the average sensitivity improves by the factor of 26.18% in comparison with the nonoverlap window, by choosing the sliding step equal to *n*/3. Whereas, the obtained average sensitivity, when the sliding step is equal to *n*/10, improves approximately 0.83% compared to the situation that the sliding step is chosen *n*/3. Based on this observation, we have selected the sliding step of *n*/3 in our proposed algorithm for the remaining processes. Figures 3 depict the final results of the proposed algorithm applied on the ten dermatoscopic samples. In all of these figures, we have selected the window length and the sliding step equal to *n* = 100 and *n*/3, respectively.

To prove the generality of the proposed algorithm in the melanoma lesion segmentation, we compared it with the other tested methods including the local Otsu thresholding, LRT without overlap, discrete wavelet transform with Haar mother wavelet, and global RT. All the tested algorithms were implemented under the same conditions, as the preprocessing step is similar for all them. In Table 2, the quantities of precision, sensitivity, specificity, and *AC* represent for the 38 dermatoscopic samples with the melanoma lesion. These parameters are also shown in Figure 4. As it is obvious, the sensitivity and *AC* improve by the factor of 2.64 (1.48), 1.34 (1.20), 1.23 (2.05), and 1.11 (1.02) in our proposed algorithm compared to the global RT, LRT without overlap, local Otsu thresholding, and discrete wavelet transform methods, respectively. As it can be seen from Figure 4, two methods, the LRT without overlap and local Otsu thresholding, are superior compared to the global RT. To be specifically in the case of employing the global RT to obtain the optimal threshold level, the melanoma lesion is not recognized in the six dermatoscopic samples. This phenomenon confirms that selecting a threshold level alone is not appropriate for the entire DI. In the proposed algorithm, the angle lines are orientated similar to the discrete wavelet transform approach. Furthermore, by converting the image into the binary version and applying the overlapping windows, the melanoma recognition rate is improved, as it can be observed from Table 2.

The proposed algorithm is applied on the ten dermatoscopic samples without melanoma lesion and the results are shown in Figure 5. Furthermore, the average quantities

Table 2: Quantitative values of accuracy, sensitivity, specificity, and approximation correlation for 38 dermatoscopic samples containing melanoma lesion

	Accuracy (%)	Sensitivity (%)	Specificity (%)	AC (%)
Radon	95.69	35.84	99.56	61.27
Local Radon without overlap	96.82	70.51	99.12	76.00
Local Otsu thresholding	98.07	76.94	99.82	86.38
DWT	98.83	84.98	99.55	88.94
Proposed method	98.81	94.85	99.23	90.99

AC – Approximation correlation; DWT – Discrete wavelet transform

Table 3: Quantitative values of accuracy, sensitivity, specificity, and approximation correlation for 38 dermatoscopic samples without melanoma lesion

	Accuracy (%)	Sensitivity (%)	Specificity (%)	AC (%)
Local Radon without overlap	97.95	68.75	99.36	74.36
Local Otsu thresholding	98.60	72.61	99.83	81.41
DWT	99.14	67.64	99.87	70.92
Proposed method	98.92	89.51	99.35	86.06

AC – Approximation correlation; DWT – Discrete wavelet transform

of precision, sensitivity, specificity, and *AC* related to the whole 38 dermatoscopic samples are depicted in Table 3 and Figure 6. The amounts of sensitivity and *AC* in our proposed algorithm improve by the factors of 1.30 (1.15), 1.23 (1.05), and 1.21 (1.32) in comparison with the LRT without overlap, local Otsu thresholding, and discrete wavelet transform methods, respectively. Note that, the functionality of the discrete wavelet transform approach is lower than the other methods in recognizing the nonmelanoma lesion; whereas as we discussed previously, this method outperformed the other tested approaches in the melanoma lesion diagnosis. The reason of this discrepancy refers to the prominent borders of the melanoma lesions. From Table 3, we can conclude that the performance of the proposed algorithm is more suitable for the images with the melanoma lesion compared to the nonmelanoma one. The main advantage of the proposed algorithm is its robustness against the discrepancy in the skin texture, skin color, presence or absence of hair, and even the weak or strong borders on the skin, for both the melanoma and nonmelanoma DIs.

Figures 7 and 8 show the extracted features, symmetry (A), border (B), color (C), diameter (D), and the TDS criteria, for both the dermatoscopic samples with (out) melanoma, respectively. The amounts of TDS for the four-selected samples of Figures 7 and 8 are 10.35 (4.37), 6.88 (2.74), 7.71 (3.01), and 8.28 (4.57), respectively. Table 4 shows the number of samples diagnosed as the benign, suspicious, and melanoma lesions in the DIs with melanoma that are labeled as malignant lesions. Similarly, Table 5 depicts the number of samples diagnosed as the benign, suspicious, and melanoma lesions in the DIs without melanoma that are labeled as benign lesions. The number of corrected samples in these two states for the proposed algorithm, discrete wavelet transform, local Otsu thresholding, and LRT without overlap are 28 (26), 25 (20), 24 (24), and 20 (22), respectively. Figures 9-11 depict the designed user-friendly software package to classify the skin lesions into the benign, suspicious, and melanoma ones. These packages were designed in MATLAB environment and performed on a computer with a 1.6 GHz processor and 8 GB random-access memory. In these packages, extraction of ABCD features is done separately and the amount of TDS criteria is calculated automatically for each image, and eventually, the result is announced as a separate message.

Table 4: The number of samples diagnosed as the benign, suspicious, and melanoma lesions based on the total dermoscopy score criteria in the dermatoscopic images with melanoma that are labeled as malignant lesions

Dataset_1 (melanoma)	Benign skin lesion	Suspicious	Melanoma
Local Radon without overlap	13/38	5/38	20/38
Local Otsu thresholding	14/38	0/38	24/38
DWT	11/38	2/38	25/38
Proposed method	8/38	2/38	28/38

DWT – Discrete wavelet transform

Table 5: The number of samples diagnosed as the benign, suspicious, and melanoma lesions based on the total dermoscopy score criteria in the dermatoscopic images without melanoma that are labeled as benign lesions

Dataset_2 (not melanoma)	Benign skin lesion	Suspicious	Melanoma
Local Radon without overlap	22/38	3/38	13/38
Local Otsu thresholding	24/38	6/38	8/38
DWT	20/38	0/38	18/38
Proposed method	26/38	4/38	8/38

DWT – Discrete wavelet transform

Conclusion

In this article, an efficient algorithm including preprocessing, main processing, and refinement procedure stages was proposed to diagnose the melanoma lesions in the DIs. In the main processing step, by applying the LRT algorithm as well as correctly detection of the angle of the melanoma border, the best threshold level was captured to binarize the image. The main advantage of the proposed algorithm is its robustness against the discrepancy in the skin texture and presence or absence of hair, for both the melanoma and nonmelanoma DIs. The inability of diagnosing the lesions with the similar color intensities in the border and background regions is one of the restrictions of the proposed algorithm.

Acknowledgment

Safadasht Branch, Islamic Azad University, is gratefully acknowledged.

Financial support and sponsorship

This study was financially support by Safadasht Branch, Islamic Azad University.

Conflicts of interest

There are no conflicts of interest.

References

- Jemal A, Siegel R, Ward E, Hao Y, Xu J, Murray T, *et al.* Cancer statistics, 2008. *CA Cancer J Clin* 2008;58:71-96.
- Argenziano G, Soyer H, De Giorgi V. *Dermoscopy: A Tutorial*. Milan, Italy: EDRE Medical Publishing and New Media; 2002.
- Steiner A, Binder M, Schemper M, Wolff K, Pehamberger H. Statistical evaluation of epiluminescence microscopy criteria for melanocytic pigmented skin lesions. *J Am Acad Dermatol* 1993;29:581-8.
- Binder M, Schwarz M, Winkler A, Steiner A, Kaider A, Wolff K, *et al.* Epiluminescence microscopy. A useful tool for the diagnosis of pigmented skin lesions for formally trained dermatologists. *Arch Dermatol* 1995;131:286-91.
- Ramezani M, Karimian A, Moallem P. Automatic detection of malignant melanoma using macroscopic images. *J Med Signals Sens* 2014;4:281-90.
- Emre Celebi M, Alp Aslandogan Y, Stoecker WV, Iyatomi H, Oka H, Chen X, *et al.* Unsupervised border detection in dermoscopy images. *Skin Res Technol* 2007;13:454-62.
- Fondn I, Serrano C, Acha B. Segmentation of Skin Cancer Images Based on Multistep Region Growing. *MVA2007 IAPR Conference on Machine Vision Applications*; 2007. p. 339-42.
- Amalian B, Fatichah C, Widyanto MR. ABCD feature extraction for melanoma skin cancer diagnosis. In: *Proceedings of the 9th International Conference on Advanced Computer Science and Information System*; 2009. p. 224-8.
- Smaoui N, Bessassi S. A developed system for melanoma diagnosis. *Int J Comput Vis Signal Process* 2013;3:10-7.
- Grana C, Pellacani G, Cucchiara R, Seidenari S. A new algorithm for border description of polarized light surface microscopic images of pigmented skin lesions. *IEEE Trans Med Imaging* 2003;22:959-64.
- Ammara M, Al-Jumaily AA. Fuzzy C. Mean thresholding based level set for automated segmentation of skin lesions. *J Signal Inf Process* 2013;4:66-71.
- Rubegni P, Ferrari A, Cevenini G, Piccolo D, Burrioni M, Perotti R, *et al.* Differentiation between pigmented spitz naevus and melanoma by digital dermoscopy and stepwise logistic discriminant analysis. *Melanoma Res* 2001;11:37-44.
- Zhou H, Schaefer G, Celebi ME, Lin F, Liu T. Gradient vector flow with mean shift for skin lesion segmentation. *Comput Med Imaging Graph* 2011;35:121-7.
- Stoecker WV, Wronkiewicz M, Chowdhury R, Stanley RJ, Xu J, Bangert A, *et al.* Detection of granularity in dermoscopy images of malignant melanoma using color and texture features. *Comput Med Imaging Graph* 2011;35:144-7.
- Dalila F, Zohra A, Reda K, Hocine C. Segmentation and classification of melanoma and benign skin lesions. *Optik (Stuttg)* 2017;140:749-61.
- Zhang X. Melanoma segmentation based on deep learning. *Comput Assist Surg (Abingdon)* 2017;22:267-77.
- Pennisi A, Bloisi DD, Nardi D, Giampetruzzi AR, Mondino C, Facchiano A, *et al.* Skin lesion image segmentation using Delaunay triangulation for melanoma detection. *Comput Med Imaging Graph* 2016;52:89-103.
- Ma Z, Tavares JM. A novel approach to segment skin lesions in dermoscopic images based on a deformable model. *IEEE J Biomed Health Inform* 2016;20:615-23.
- Fdhal N, Kyan M, Androustos D, Sharma A. Color space transformation from RGB to CIELAB using neural networks. In: Muneesawang P, Wu F, Kumazawa I, Roeksabutr A, Liao M, Tang X, editors. *Advances in Multimedia Information Processing-PCM 2009: Lecture Notes in Computer Sciences*. Vol. 5879. Berlin, Heidelberg: Springer; 2009.
- Johari M, Esmaeili F, Andalib A, Garjani S, Saberkari H. A novel thresholding based algorithm for detection of vertical root fracture in nonendodontically treated premolar teeth. *J Med Signals Sens* 2016;6:81-90.
- Singh RP, Dixit M. Histogram equalization: A strong technique for image enhancement. *Int J Signal Process Image Process Pattern Recognit* 2015;8:345-52.
- Shao G, Li T, Zuo W, Wu S, Liu T. A combinational clustering based method for cDNA microarray image segmentation. *PLoS One* 2015;10:e0133025.
- Bariamis D, Iakovidis DK, Maroulis D. M3G: Maximum margin microarray gridding. *BMC Bioinformatics* 2010;11:49.
- Pourreza R, Banaee T, Pourreza H, Kakhki RD. A radon transform based approach for extraction of blood vessels in conjunctival images. In: Gelbukh A, Morales EF editors. *Mexican International Conference on Artificial Intelligence 2008, Lecture Notes in Artificial Intelligence 5317*; 2008. p. 948-56.
- Stolz W. ABCD rule of dermatoscopy: A new practical method for early recognition of malignant melanoma. *Eur J Dermatol* 1994;4:521-7.
- Amelard R, Glaister J, Wong A, Clausi DA. High-level intuitive features (HLIFs) for intuitive skin lesion description. *IEEE Trans Biomed Eng* 2015;62:820-31.

BIOGRAPHIES



Alireza Amoabedini received his B.Sc. in Computer Engineering from the Islamic Azad University Branch of Kashan, Iran, in 2007. He received his M.Sc. in IT Engineering from Sharif University of Technology, Iran in 2010. Since 2013, he is a Ph.D. student in IT Engineering (Network) in Faculty of New Sciences and Technology,

University of Tehran. He is a scientific member of faculty of Computer Sciences in Islamic Azad University Branch of Safadasht, Tehran, Iran, since 2012. His research interests include Molecular Communication, Information Technology in Medicine, Computer Networks, Biomedical image processing, bioinformatics, and pattern recognition, Network Security, Intelligent Transportation Systems (ITS), Wireless Sensor Networks.

Email: amoabedini@safaiu.ac.ir



Mahsa Saffari Farsani was born in Shahrekord, Iran, in 1989. She received the B.Sc. degree in Electrical Engineering from the University of Shahrekord, Shahrekord, Iran. In 2015, she received the M.Sc. degree in Communication Engineering from Yazd University, Yazd, Iran. Her research interests include biomedical

image processing, bioinformatics, and pattern recognition

Email: m.saffari@stu.yazd.ac.ir



Hamidreza Saberkari received his B.Sc. in Electrical Engineering from the University of Guilan, Rasht, Iran, in 2011. In 2013, he received his M.Sc. in Communication Engineering from Sahand University of Technology, Tabriz, Iran. In 2016, he received his PhD degree in Electrical Engineering from Sahand University of

Technology, Tabriz, Iran. His research interests include biomedical image processing, bioinformatics, and pattern recognition.

Email: h_saberkari@sut.ac.ir



Ehsan Aminian received the M.S. degree from Islamic Azad University, Science & Research branch, Tehran, Iran, in 2009. He is the director of engineering department of Azad University, Safadasht branch. His current research interests include machine learning, pattern recognition and data mining.

Email: Ehaminian@gmail.com